THE JOURNAL OF PHYSICAL CHEMISTRY C

Article

Cite This: J. Phys. Chem. C 2018, 122, 26623−26634

pubs.acs.org/JPCC

Integral Method Analysis of Electroabsorption Spectra and Electrophotoluminescence Study of $(C_4H_9NH_3)_2PbI_4$ Organic−Inorganic Quantum Well

Vidya Kattoor,[†,‡,∥] Kamlesh Awasthi,[†,∥] Efat Jokar,[†] Eric Wei-Guang Diau,*[,†,§] and Nobuhiro Ohta*[,†,§]

[†]Department of Applied Chemistry and Institute of Molecular Science and [§]Center for Emergent Functional Matter Science, National Chiao Tung University, 1001 Ta-Hsueh Rd., Hsinchu 30010, Taiwan

[‡]Sustainable Chemical Science and Technology (SCST), Taiwan International Graduate Program (TIGP), Academia Sinica, Nankang, Taipei 115, Taiwan

Supporting Information

ABSTRACT: Electric-field-induced changes in absorption and photoluminescence (PL) spectra and in PL decay profile have been measured for two-dimensional hybrid organic−inorganic halide perovskite semiconductor, $((C_4H_9NH_3)_2PbI_4)$ (N1). Electroabsorption (E-A) spectra observed at room temperature and at a low temperature of 45 K were analyzed by assuming the Stark shift, and the magnitudes of the change in electric dipole moment and polarizability following photoexcitation were determined. The strong signal observed in the E-A spectra at 45 K was interpreted in terms of the weak absorption band which shows extremely large Stark shift resulting from the large change in polarizability following photoexcitation. Electrophotoluminescence spectra of this compound, that is, field-induced change in PL spectra, show that PL of N1 is quenched by the application of electric field. Field effects on PL decay profiles show that the quenching results both from the field-induced decrease of the population of the emitting state following photoexcitation and from the field-induced lifetime shortening caused by the enhancement of the nonradiative decay rate at the emitting state. At a low temperature of 45 K, two exciton emissions, each of which originates from different phase, appear, and both emissions are quenched by the applied electric field with different efficiencies from each other. It is also found that trap emissions observed at low temperature in the wavelength region longer than the sharp exciton bands show more efficient field-induced quenching than that of the exciton emissions, suggesting that energy transfer from the photoexcited state to trapped states is decelerated by the applied electric field.

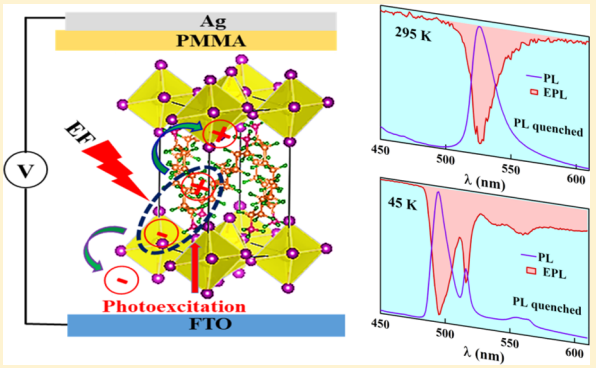

INTRODUCTION

Hybrid metal halide perovskites have attracted tremendous attention to photovoltaics and other optoelectronic applications because of their unique optical and electronic properties.[1] Besides the low cost and ease of fabrication, the wide-range tunability in structure highlights its importance.[2−8] A large number of lead-halide-based perovskites are self-organized low-dimensional materials, in which $[PbX_6]$ octahedral forms zero-, one-, two-, or three-dimensional networks.[9,10] The PbX_6^{4-} octahedra can share all its corners to form three-dimensional (3D) crystals with the stoichiometry of PbX_3^- and balance the charge by an organic cation, as $CH_3NH_3^+$ (MA). When the octahedra self-assemble into layered crystals with PbX_6^{4-} corner-sharing into a plane, a two-dimensional (2D) layer of stoichiometric PbX_6^{4-} is formed. The formed 2D layer's charge is balanced by the large-size organic cations such as $C_4H_9NH_3^+$ (BA); this type of perovskite is addressed as the 2D perovskite. The structure of 2D and 3D can merge together; the thickness of the lead iodide layer is controlled by the stoichiometric ratio of two amines. With increasing molar ratio of MA/BA cations, two (n = 2), three (n = 3), or more lead iodide octahedral layers are obtained. These structure formulates with $BA_2(MA)_{n-1}Pb_nX_{3n+1}$, where the integer n represents the number of inorganic perovskite layers between two large-size organic cations. The value of n defines the degree of quantum and dielectric confinement as well as the optical band gap and exciton binding energy.[11] The band gap depends on the number of inorganic layers as well as the organic barrier layers.[12,13]

The photoinduced excitons and charge carriers in 2D perovskite materials confine to monomolecular layers of $[PbX_6]$ sandwiched between two organic layers. Another

Received: August 21, 2018
Revised: October 23, 2018
Published: November 8, 2018

DOI: 10.1021/acs.jpcc.8b08116
J. Phys. Chem. C 2018, 122, 26623−26634

interesting feature of the 2D materials is that the dielectric constant of inorganic layer is higher than that of the organic layer, which tends to significantly increase coulomb interaction between the electron and holes in the inorganic layer.[14−16] Thus, the above-mentioned properties make 2D perovskite as a critical racer for functional devices such as light-emitting diodes, field-effect transistors, and hard radiation detectors.[17−19] The 2D compounds with n value one, two, three, and so forth, and butyl ammonium as organic cations have been a hot topic for the applied and basic research.[20−23] In the similar vein, the excitonic and electronic properties of various 2D perovskites have been studied by the electroabsorption (E-A) spectroscopy and two photon absorption spectroscopy.[18,24−26]

External electric-field effects on absorption and photoluminescence (PL) spectra have been extensively used to examine electronic structure as well as excited-state dynamics, following photoexcitation including electron and/or hole mobility.[26−37] Recently, E-A spectroscopic study of $(C_4H_9NH_3)_2PbI_4$ was reported by Amerling et al.[26] who fabricated the transparent thin film of $(C_4H_9NH_3)_2PbI_4$ on quartz substrate decorated with gold interdigitated electrodes and applied electric fields parallel to the inorganic $[PbI_6]^{4-}$ sheets. They focused mainly to the band-edge region to estimate the binding energy of the exciton and insisted as the first evidence for Franz−Keldysh (F−K) oscillation in $(C_4H_9NH_3)_2PbI_4$ quantum well. Because such an interpretation of the E-A spectra of 2D perovskite films is different from the ones reported so far,[25] the evidence is necessary to be carefully verified to give a reasonable interpretation for the E-A spectra. In the present study, $(C_4H_9NH_3)_2PbI_4$ organic inorganic 2D perovskite crystal, which is hereafter denoted by N1, has been synthesized. Then, external electric field was applied perpendicular to the inorganic $[PbI_6]^{4-}$ layer to measure E-A spectra of N1 at 295 K and at 45 K, in contrast with the experiments in ref 26, where electric field was applied parallel along the $[PbI_6]^{4-}$ layer. E-A spectra of N1 films show a large signal in the region between the first and second exciton bands at 45 K. This signal could not be reproduced by the so-called differential method analysis. Then, the E-A spectra were analyzed by the so-called integral method, and unknown weak absorption band has been proposed to be located in N1 thin films between the first and second strong absorption bands. Note that the integral method can be used to analyze E-A spectra, even when the E-A spectra show the intense signal beyond the identified absorption bands, where the typical differential method analysis become unsatisfactory or failed to simulate the E-A spectra.[38,39] In the result, E-A spectra have been interpreted in terms of the Stark shift in the whole spectral region, and the magnitude of the change in electric dipole moment and/or polarizability following the absorption into the bands of N1 thin films has been estimated at 295 and 45 K.

In addition to the E-A measurements, electrophotoluminescence (E-PL) spectra of N1 thin films, that is, electric-field-induced changes in PL spectrum, have been measured for N1 thin films. Besides the E-PL spectra at room temperature and at 45 K, field-induced changes in the PL decay profile have also been measured at room temperature. On the basis of these results, carrier dynamics and relaxation of exciton following photoexcitation of N1 both in the absence and in the presence of electric field have been discussed.

EXPERIMENTAL SECTION

Synthesis of $(C_4H_9NH_3)_2PbI_4$ (N1) 2D perovskite crystals was performed based on the previously reported procedure.[40] For the synthesis, PbO powder (2232 mg, 10 mmol) was dissolved in a mixture of HI solution (10.0 mL, 76 mmol) and 50% aqueous H_3PO_2 (1.7 mL, 15.5 mmol) at room temperature. The obtained yellow solution was heated until boiled condition and kept stirred under constant magnetic stirrer for about 5 min. Neutralized *n*-butylamine (924 μL, 10 mmol) with HI 57% w/w (5 mL, 38 mmol) was added to the PbI_2 solution. The stirring of boiled solution was discontinued, and the solution was left to cool down to room temperature. After 2 h, the obtained orange rectangular-shaped plates were collected by suction filtration and dried in a vacuum oven at room temperature. The N1 2D perovskite thin films were prepared on a fluorine-doped tin oxide (FTO)-coated glass substrate by hot casting method. The FTO-coated substrate was preheated at 120 °C for 10 min, and then 0.05 mM solution of 2D perovskite was spin-coated on the preheated FTO glass. Thickness of the homogeneous N1 films was about ∼130 ± 10 nm. Then, a poly(methyl methacrylate) (PMMA) film was deposited on the N1 film by a spin-coating method. The typical thickness of the films was ∼0.7 μm, which was determined by using alpha step method (Veeco Dektak 150), and the strength of the applied electric field was estimated as the applied voltage divided by thickness. A semi-transparent Ag film with a thickness of ∼30 nm was further deposited on the PMMA film through the thermal deposition. FTO and Ag films served as electrodes for the E-A and E-PL measurements. The growth direction of the film which corresponds to the $[PbI_6]^{4-}$ layers in N1 thin films is perpendicular to the FTO substrate, that is, the electric field was applied parallel to the growth direction.

All of the optical measurements were performed under vacuum condition. Steady-state absorption and PL spectra were recorded with a fluorescence spectrometer (JASCO, FP-777). Electric-field modulation spectroscopy was applied to measure E-A and E-PL spectra, with the same apparatus as described elsewhere.[41] A modulation in transmitted light intensity of the excitation light and in PL intensity were induced by application of the sinusoidal ac voltage with a modulation frequency of 40 Hz. Field-induced change in transmitted light intensity of excitation light or PL intensity (I_{PL}) was detected with a lock-in amplifier at the second harmonic of the modulation frequency. The dc component of the transmitted excitation light intensity or PL intensity was measured simultaneously, along with the modulated signal induced by the applied electric field. E-A spectra and E-PL spectra were obtained by plotting field-induced change in absorbance (ΔA) and field-induced change in PL intensity (ΔI_{PL}) as a function of wavelength or wavenumber, respectively. The temperature-dependence measurements were performed by using a cryogenic refrigerating system (Daikin, V202C5LR) equipped with quartz optical windows. The temperature of the substrate was controlled and monitored by using a temperature controller system (Scientific Inst. model 9600) equipped with a silicon diode thermometer.

RESULTS AND DISCUSSION

Absorption and E-A Spectra. Figure 1a,b shows the normalized optical absorption and PL spectra of N1 at 295 and 45 K. Figure 1c shows the X-ray diffraction pattern of N1, and

DOI: 10.1021/acs.jpcc.8b08116
J. Phys. Chem. C 2018, 122, 26623−26634

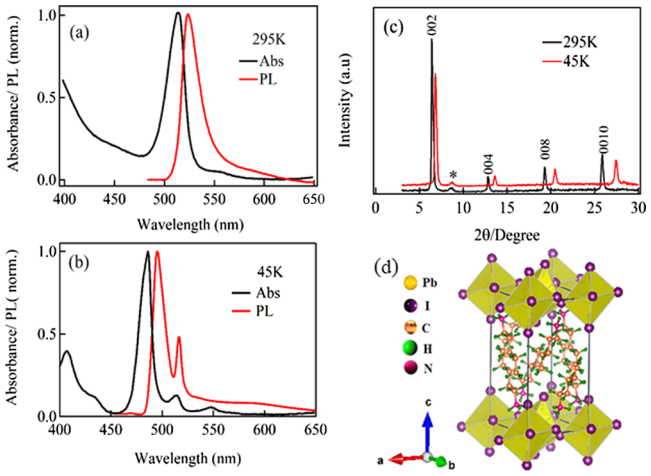

Figure 1. (a) Normalized optical absorption and PL spectra of $(C_4H_9NH_3)_2PbI_4$ (N1) 2D perovskite thin film at 295 K, (b) absorption and PL spectra of N1 at 45 K, (c) XRD pattern of N1 thin film at 295 K and at 45 K, where the peak assigned by "*" is related to the equipment, and (d) unit cell and crystal structure of 2D perovskite of N1 film.

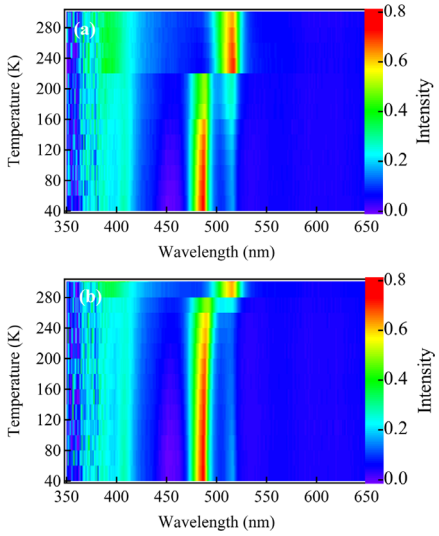

Figure 2. Map of the temperature-dependent absorption intensity of N1 2D perovskite obtained by cooling temperature from 295 K (a) and by heating the temperature from 40 K (b).

Figure 1d shows the corresponding crystal structure. Prominent exciton and PL peaks were observed for N1 thin films at both temperatures. The absorption of N1 thin film at 295 K which shows one main exciton absorption band at 515 nm (Figure 1a) is assigned to the 1s exciton. This band was assigned to the intra-atomic transition from the 6*s* to 6*p* orbital in Pb^{2+},[42,43] and the large binding energy and large oscillator strength of this band were explained in terms of the dielectric confinement effect. "*p*" orbital has three-levels split by the crystal field and spin−orbit interaction and exhibits less dispersion than "*s*". Later, this 1s band was reassigned to the interatomic transition from the iodine atom to the lead atom.[44] If this 1s band has a character of interatomic charge transfer, a large change in electric dipole moment may be expected following absorption.

Absorption spectrum of N1 depends on the temperature. Figure 2 shows the map of the temperature-dependent absorption intensity, and absorption spectra at various temperatures are shown in Supporting Information (Figures S1 and S2). As the temperature decreases from room temperature, the intensity of the main absorption peak at ∼515 nm slightly increases but suddenly decreases below 200 K, and a new peak appeared at 486 ± 2 nm, with a 30 nm blue shift. Along with the peak at ∼486 nm, well-structured three absorption bands were observed in the wavelength region below 450 nm. The drastic change in the absorption spectra which occurs at around 200 K probably comes from the structural change of butyl ammonium chain.[45,46] Then, the strong band at 486 nm observed at low temperatures may be assigned to the 1s exciton in the new phase produced by phase transition at low temperatures. The phase at high temperature and at low temperature is denoted by H-phase and L-phase, respectively.[47] Hereafter, the broad absorption band at ∼445 nm observed at very low temperature, for example, at 45 K is hereafter presented as α band, and much higher energy bands are called as β and γ bands, respectively. Because of the crystal field and the spin−orbit interaction, the threefold degeneracy in the conduction band lifts into three bands.[21] In the present absorption region, the optical transitions from the topmost valence band to these conduction bands have to be considered. In $(C_{10}H_{21}NH_3)_2PbI_4$, for example, the absorption bands in the region of 3−3.5 eV, that is, 24 000−28 000 cm^{-1}, are considered to be different from the 1s band,[10] in the sense that the reached conduction bands are different from each other. As mentioned later, not only the β and γ bands but also the α band in N1 may correspond to the conduction band which is different from the one of the 1s exciton, although the α band was assigned to the 2s exciton,[48] which corresponds to the same conduction band as the 1s exciton. Extra absorption feature at around 550 nm observed at low temperature at 45 K may suggest the occurrence of a more disordered energetic structure.

When the temperature increased from 40 K, absorption spectra returned to the original spectrum at room temperature. As shown in Figure 2, however, the phase-transition temperature is different from the one observed in the experiments where the temperature was decreased from 295 K; the peak at 486 nm appears at 260 K by heating from 40 K, whereas this peak disappears at 200 K by cooling from 295 K, indicating the presence of hysteresis in the map of temperature-dependent absorption intensity. Even at low temperatures below 100 K, weak absorption peak is observed at ∼515 nm besides the strong band at 486 nm, implying that the phase similar to the one which is dominant at high temperature at 295 K still exists a little at the low temperature.

Note that the temperature-dependent absorption spectra obtained by cooling from room temperature and by heating from 40 K are shown in the Supporting Information (Figures S1 and S2).

The X-ray diffraction (XRD) patterns obtained at 295 and 45 K shown in Figure 1c indicate that the shift of the temperature-dependent absorption peak does not come from the phase transition of the crystal structure; the crystal structure of N1 having an orthorhombic structure at room temperature remains unchanged even after the phase transition at low temperatures. The Braggs peaks at 45 K shifted to a higher value of diffraction angle, which means that the lattice contraction which induces decreases of the inter-inorganic slab spacing occurs at low temperatures.[49] The temperature-dependent absorption peak shift which occurs at 200−260 K

DOI: 10.1021/acs.jpcc.8b08116
J. Phys. Chem. C 2018, 122, 26623−26634

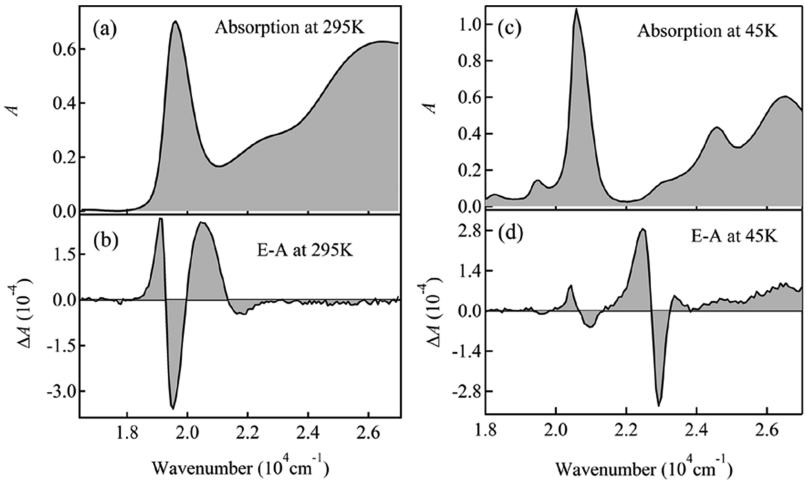

Figure 3. Absorption spectra (upper) and E-A spectra (lower) of N1 at 295 K (left) and at 45 K (right); the E-A spectra were obtained with a field strength of 0.4 MV cm^{-1}.

comes from the rearrangement of butyl ammonium chains at low temperatures, as mentioned already. At room temperature, the butyl ammonium chains adopt trans conformation. However, the decrease in temperature induces changes in butyl chain conformation, and the structural changes are characterized by a decreased conformational disorder of the methylene units of the butyl chains and gain of tilt angle coherence leading to a decrease in the inter-slabs spacing.

E-A spectra of N1 thin films were observed at 295 K and at 45 K with different field strengths in the range of 0.2−0.4 MV cm^{-1}, as shown in the Supporting Information (Figure S3 for 295 K and Figures S4 and S5 for 45 K). The results obtained with a field strength of 0.4 MV cm^{-1} are shown in Figure 3, together with the absorption spectra. E-A spectra of N1 at room temperature and at 50 K were also reported by Amerling et al.[26] It may be important to note that the applied field directions are opposite to each other; the applied field direction was perpendicular to the growth direction of $[PbI_6]^{4-}$ in their experiments, whereas the field direction was parallel to the growth direction in the present experiments, as mentioned in the Experimental Section. The present E-A spectra look similar to their spectra, except that our prominent E-A peak located at 20 510 cm^{-1} at room temperature and at 22 315 cm^{-1} at low temperature is less enhanced. It is not certain whether the difference comes from the applied-field-direction dependence and/or some difference in sample condition. They explained that the E-A signal of the exciton bands results from the Stark shift. In addition, the band gap modulation at 50 K was reported to be dominated by the F−K oscillation, based on the $F^{1/3}$ peak amplitude dependence and the E-A oscillatory response broadening with the field. It was mentioned that the F−K oscillation was not clearly visible at room temperature. In the present experiments, it was confirmed that the E-A signal at room temperature was proportional to the square of the applied electric field, as shown in Figure 4. It was also confirmed that the E-A signal of the prominent peaks at 22 315 and 22 920 cm^{-1} (2.77 and 2.84 eV, respectively) at 45 K was proportional to the square of the applied electric field, as shown in Figure 4, indicating that the main peaks of the E-A spectra observed both at 295 K and at 45 K are caused by the Stark shift.[50] Only at around 23 350 cm^{-1}, the E-A spectra observed at 45 K cross the zero line of ΔA at different wavenumbers (see Figure S5), which was also

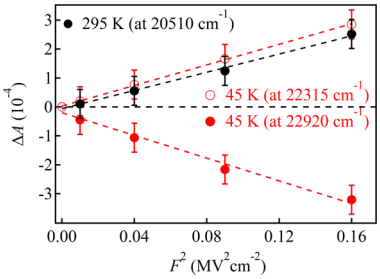

Figure 4. Plots of electric-field-induced change in absorption intensity of N1 thin films at 295 and 45 K, as a function of the square of the applied electric field strength.

reported in ref 26. In other regions, the E-A spectra observed with different applied field strengths were essentially the same in shape both at 295 and 45 K (see Figures S3−S5 in the Supporting Information). On the basis of these results, the observed E-A spectra were analyzed in terms of the Stark effect, that is, in terms of field-induced spectral shift and broadening, as mentioned below.

In the presence of the electric field, the energy of the absorption band is shifted by $-\Delta\boldsymbol{\mu} - \Delta\boldsymbol{\alpha}F^2/2$, where $\Delta\boldsymbol{\mu}$ and $\Delta\boldsymbol{\alpha}$ represent the change in electric dipole moment and polarizability, respectively, between the excited state (e) and ground state (g), that is, $\Delta\boldsymbol{\mu} = \boldsymbol{\mu}_e - \boldsymbol{\mu}_g$ and $\Delta\boldsymbol{\alpha} = \boldsymbol{\alpha}_e - \boldsymbol{\alpha}_g$. Then, the field-induced change in absorption intensity at wavenumber, ν, observed at the second harmonic of modulation frequency, that is, $\Delta A(\nu)$ is considered to be given by a sum of the zeroth, first, and second derivatives of the absorption intensity $A(\nu)$, as follows[35,51−53]

$$\Delta A(\nu) = (fF)^2\left[A_\chi A(\nu) + B_\chi \nu \frac{d}{d\nu}\left(\frac{A(\nu)}{\nu}\right) + C_\chi \nu \frac{d^2}{d\nu^2}\left(\frac{A(\nu)}{\nu}\right)\right] \quad (1)$$

Here, $F = |\boldsymbol{F}|$ and f is the internal field factor. The nonzero coefficient of the zeroth-derivative term comes from the field-induced change in transition moment, and the coefficients B_χ and C_χ correspond to the spectral shift and spectral broadening of the absorption bands, which mainly result from $\Delta\boldsymbol{\alpha}$ and $\Delta\boldsymbol{\mu}$,

DOI: 10.1021/acs.jpcc.8b08116
J. Phys. Chem. C 2018, 122, 26623−26634

respectively, following absorption. The magnitude of $\Delta\boldsymbol{\alpha}$ and $\Delta\boldsymbol{\mu}$ can be calculated through the given relations

$$B_\chi = \frac{\Delta\bar{\alpha}}{2hc}, \qquad C_\chi = \frac{|\Delta\boldsymbol{\mu}|^2}{6h^2c^2} \tag{2}$$

Here, $\Delta\bar{\alpha}$ denotes the trace of $\Delta\boldsymbol{\alpha}$, that is, $\Delta\bar{\alpha} = (1/3)\mathrm{Tr}(\Delta\boldsymbol{\alpha})$.

In the absorption spectra at 295 K, a small shoulder located in the higher wavenumber region of the 1s band may be assigned to a phonon side band.[54] The E-A spectrum at 295 K in the wavenumber region below 21 000 cm^{-1} can be reproduced quite well by a linear combination of the derivative components of the 1s band and the phonon side band, denoted by 1_{ss}, according to eq 1, that is, with the differential method by assuming the Gaussian profile for these two absorption bands. The results are shown in the Supporting Information (Figure S6). The fact that the shape of the E-A spectrum at 295 K is very similar to the second derivative of the 1s band indicates that the change in electric dipole moment, $\Delta\boldsymbol{\mu}$, is significant following the 1s absorption of the H-phase. In the wavenumber region of 21 000−23 000 cm^{-1}, however, the E-A spectrum at room temperature could not be reproduced well by the differential method (see Figure S6); clear absorption band cannot be identified in the region between the 1_{ss} band at 20 430 cm^{-1} and the band having a peak at 22 500 cm^{-1}, where clear E-A signal was observed. It is also known that absorption bands located at wavenumbers higher than 23 000 cm^{-1} have no significant contribution of the first and second derivative components of the absorption bands in the E-A spectra, except for the slight decrease of the absorption intensity in the presence of the applied electric field.

In contrast with the E-A spectrum at 295 K, the E-A spectrum at 45 K around the 1s exciton band is very similar in shape to the first derivative spectrum of the 1s band (see Figure S7 of the Supporting Information), implying that the field-induced change in absorption spectrum of the 1s band of the L-phase mainly comes from $\Delta\boldsymbol{\alpha}$ following absorption. In fact, the E-A spectrum around the 1s band at 45 K can be reproduced by the differential method, that is, by a linear combination of zeroth, first, and second derivative components, as shown in the Supporting Information (Figure S7). Higher exciton bands located at wavenumbers more than 24 000 cm^{-1} show the field-induced enhancement in intensity, in contrast with the E-A spectrum at 295 K. Further, there is no doubt that E-A spectrum in the region of 21 300−23 500 cm^{-1} at 45 K, that is, in the region between the 1s exciton and the α band, where strong E-A signal was observed, cannot be reproduced by the differential method because clear absorption band(s) cannot be identified in this region (see Figure S7).

The fact that the E-A spectrum both at 295 K and at 45 K cannot be reproduced by the differential method in the region between the 1s exciton and the α band suggests the possibility that the absorption band having a large electric-field effect, which is not identified in the observed absorption spectrum because of its very weak intensity, is located in this region. Then, the integral method analysis was used to figure out the clear picture of the origin of unsatisfactory simulations for N1.

If the experimentally observed E-A signal is given by a linear combination of the zeroth, first, and second derivatives of the absorption spectra, as shown in eq 1, the integral of the E-A spectra along with wavenumber can be approximately given as follows

$$\int \Delta A(\nu)\mathrm{d}\nu \cong (fF)^2\left[A_\chi \int A(\nu)\mathrm{d}\nu + B_\chi A(\nu) + C_\chi \frac{\mathrm{d}A(\nu)}{\mathrm{d}\nu}\right] \tag{3}$$

In the right-hand side of eq 3, the first term shows a monotonic increase or decrease, as a function of wavenumber, depending on the sign of A_χ, and the saturation occurs with the increasing wavenumber. The second term shows the spectral shape given by the absorption spectrum, and the third term shows the spectral shape given by the first derivative of the absorption spectrum. Further integration of eq 3, that is, the second integral of the E-A spectra along the wavenumber may be given as follows

$$\begin{aligned}\int\left\{\int \Delta A(\nu)\mathrm{d}\nu\right\}\mathrm{d}\nu &\cong (fF)^2\left[A_\chi \int\left\{\int A(\nu)\mathrm{d}\nu\right\}\mathrm{d}\nu + B_\chi \int A(\nu)\mathrm{d}\nu \right.\\ &\left. + C_\chi A(\nu)\right]\end{aligned} \tag{4}$$

The first and second terms in the right-hand side show a monotonic increase or decrease, depending on the sign of A_χ and B_χ, whereas the third term shows a spectral shape which is the same as the absorption spectrum.

In the integral method analysis, the first integral and the second integral of the observed E-A spectrum are taken, according to eqs 3 and 4. The results of N1 at 295 and 45 K are shown in Figures 5 and 6, respectively. Equation 4 indicates that the second integral of the E-A signal that corresponds to the second derivative of the absorption spectrum should show the spectrum whose shape is similar to the absorption spectrum. In fact, the second integral of the E-A spectrum at 295 K shows the peak which corresponds to the 1s exciton band, as shown in Figure 5c, indicating that the second derivative of the 1s absorption band gives a large contribution in the E-A spectrum. The absence of the peak in the region other than the 1s band suggests that the absorption band which gives its second derivative component is not necessary to be considered in the analysis of the E-A spectrum at 295 K, except for the 1s band. If the first derivative of the absorption band contributes to the E-A spectrum, the first integral of the E-A spectrum keeps the absorption spectrum in shape, as shown in eq 3. When the first integral of the E-A spectrum at 295 K given in Figure 5b is looked from this point of view, it is noticed that there is a peak at around 21 000 cm^{-1} in the first integral of the E-A spectrum, suggesting that a weak unknown absorption band, whose first derivative component largely contributes to the E-A spectrum, exists with a peak at ∼21 000 cm^{-1}. Hereafter, this band is represented as the X_{295} band.

The positive and negative peaks in the first integral of the E-A spectrum at around the 1s band at 295 K, which are shown in Figure 5b, originate from the first derivative of the 1s absorption band. Note that the first integral of the second derivative component in the E-A spectrum gives a shape corresponding to the first derivative of the absorption spectrum. Further, the monotonic increase of the second integral of the E-A spectrum at wavenumbers larger than 20 500 cm^{-1} at 295 K indicates the contribution of the zeroth derivative component of the 1s, 1_{ss}, and/or the X_{295} bands. In fact, the E-A spectrum and its first and second integral spectra could be simulated in the whole spectral region quite well by considering the contribution of the first and second derivatives

DOI: 10.1021/acs.jpcc.8b08116
J. Phys. Chem. C 2018, 122, 26623−26634

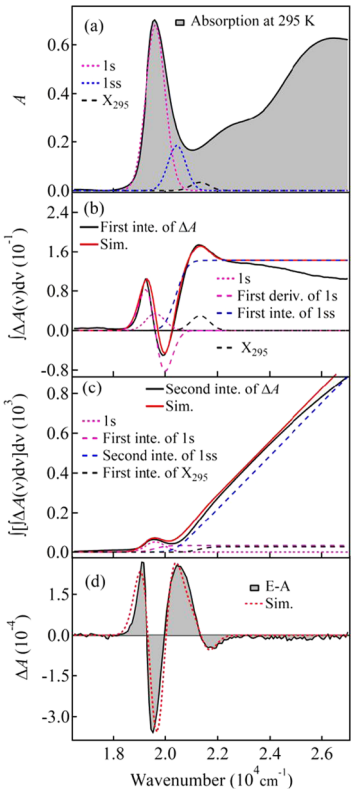

Figure 5. Integral method analysis of the E-A spectra of N1 at 295 K. (a) Absorption spectrum (shaded line) and absorption bands having a Gaussian profile, (b) first integral of the E-A spectrum (black solid line), simulated spectrum (red dotted line), and each spectral shape which contributes to the simulated spectrum, (c) second integral of the E-A spectrum (black solid line), simulated spectrum (red dotted line), and each contributed spectrum, and (d) E-A spectrum (shaded line) at a field strength of 0.4 MV cm^{-1} and the simulated spectrum (red dotted line) derived using the integral method analysis.

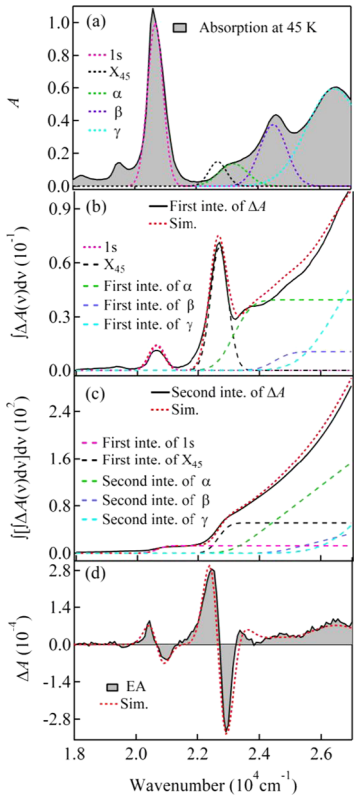

Figure 6. Integral method analysis of the E-A spectra of N1 at 45 K. (a) Absorption spectrum (shaded line) and absorption bands having Gaussian profile, (b) first integral of the E-A spectrum (black solid line), simulated spectrum (red solid line), and the spectral contribution to the simulated spectrum, (c) second integral of the E-A spectrum (black solid line), simulated spectrum (red solid line), and each spectral shape which contributes to the simulated spectrum, and (d) E-A spectrum (shaded line) at a field strength of 0.4 MV cm^{-1} and the simulated spectrum (red dotted line) derived using the integral method analysis.

of the 1s band, the zeroth derivative of the 1_{ss} band, and the first derivative of the X_{295} band, as shown in Figure 5. Note that the X_{295} band was assumed to have a Gaussian profile with a full-width at half maximum (fwhm) of 830 cm^{-1}. Actually, the electric-field effect on the absorption in the high wavenumber region is not considered in the present simulation. As shown in Figure 3b, the absorption intensity at 295 K slightly decreases in the presence of the applied electric field even in the wavenumber region above 23 000 cm^{-1}. The gradual decrease of the first integral of the E-A spectrum at 295 K as a function of wavenumber, which is not reproduced in the present simulation, is attributed to this field-induced decrease of the absorption intensity observed for the absorption in the high wavenumber region. On the basis of the simulation using the integral method, the magnitude of the field-induced change in absorption intensity, $\Delta\bar{\alpha}$ and $|\Delta\boldsymbol{\mu}|$ was determined for the 1s, 1_{ss}, and X_{295} bands at 295 K. The results are shown in Table 1. Because the X_{295} band could not be identified in the observed absorption spectrum, the exact value of $\Delta\bar{\alpha}$ following this transition could not be determined, and the value of $\Delta\bar{\alpha}$ shown in Table 1, ~200 $Å^3$, was estimated, as the minimum value by assuming that the peak intensity of this absorption band is less than 1/5 of the observed intensity at 21 340 cm^{-1}. The large value of $|\Delta\boldsymbol{\mu}|$ for the 1s band at 295 K indicates the charge-transfer characteristics of this transition, which probably comes from the interatomic transition in nature.

The above-mentioned analysis with eqs 1 and 2 is based on the assumption that the dipole moment as well as polarizability of materials are randomly oriented. Then, it may be pointed out that the layers of N1 orient parallel to the substrate, suggesting anisotropic behavior on optical and optoelectrical properties. In fact, the E-A spectra of the $(C_4H_9NH_3)_2PbBr_4$ film observed in the transverse and longitudinal configurations, where the electric fields were applied parallel to the quantum-well layers and perpendicular to the quantum-well layers, respectively, were very different in shape from each other.[24] As mentioned already, however, the present E-A spectra both at 295 K and at 45 K are very similar to the results reported in ref 26, although the directions of the applied electric fields were different from each other; fields were applied perpendicular to the substrate in the present experiments and parallel to the substrate in ref 26. Therefore, the assumption of the random orientation of materials seems to be applicable for the analysis of the present E-A spectra, although the assumption is not strict, as mentioned below.

In the present study, the E-A spectra at 295 K have been interpreted in terms of the Stark effect in the whole spectral region, that is, by considering the field-induced spectral broadening of the 1s exciton band, red-shift of the X_{295}

DOI: 10.1021/acs.jpcc.8b08116
J. Phys. Chem. C 2018, 122, 26623−26634

Table 1. Coefficients of A_χ and Magnitude of $|\Delta\mu|$ and $\Delta\bar{\alpha}$ for the Bands Contributed to the Simulated E-A Spectra of N1 at 295 K and at 45 K

temperature	transition	peak (cm^{-1})	A_χ (10^{-3} MV^{-2})	$\Delta\bar{\alpha}$ ($Å^3$)	$\lvert\Delta\mu\rvert$ (D)
295 K	1s	19 600	0	12	3.0 (±0.5)
	1_{ss}	20 430	6 (±1)	0	0
	X_{295}	21 340	0	>200 ± 50	0
45 K	1s	20 660	0	7 (±1)	0
	X_{45}	22 690	0	2410 ± 200	0
	α	23 220	1.5 (±0.5)	0	0
	β	24 500	3.2 (±1)	0	0
	γ	26 460	7.8 (±1)	0	0

band, and intensity enhancement of the phonon band (see Table 1). In ref 26, the E-A spectra observed at 300 K were interpreted in terms of the red shift caused by a change in polarizability for the 1s exciton and the band gap oscillation, but the spectral broadening of the 1s band induced by the change in electric dipole moment was not considered. The significance of the change in electric dipole moment following absorption of the 1s exciton at 295 K can be shown by the E-A spectra observed at the first harmonic of the modulation frequency, that is, the linear field effect on the absorption spectra at 295 K. As shown in the Supporting Information (Figure S8), the E-A spectra observed at the first harmonic of the modulation frequency, which depended on the applied field direction, showed the shape similar to the first derivative of the 1s exciton absorption band. These results indicate that the linear Stark shift was induced by a change in electric dipole moment along the applied field direction for the 1s band, that is, the change in electric dipole moment is involved in the E-A signal. Field-induced shift in transition energy is given by $-\Delta\mu F$, and the magnitude of $\Delta\mu$ along the applied field direction, that is, along the direction perpendicular to the substrate was estimated to be 0.03 D from the E-A spectra shown in Figure S8. At the same time, the results show that the samples were not a random-distribution system because the linear effect along the applied electric field should be cancelled to each other for dipoles whose directions are opposite to each other. However, the fact that the magnitude of $\Delta\mu$ mentioned above is about 2 orders of magnitude smaller than that derived from the E-A spectra observed at the second harmonic of the modulation frequency, that is, 3.0 D (Table 1), seems to show the validity of the approximation of the random distribution.

The above-mentioned integral method analysis was also applied to the E-A spectrum of N1 observed at 45 K because the E-A spectrum over the whole region could not be reproduced by the differential method. The E-A spectrum and its first and second integral spectra are shown in Figure 6, together with the simulated spectra. The absorption spectrum and its decomposition into each band are also shown in this figure. In the second integral of the E-A spectrum (Figure 6c), there is no clear peak, implying that the absorption band which gives the second derivative component in the E-A spectrum is not necessary to be considered. On the other hand, clear peaks appear at ~20 600 and 22 690 cm^{-1}, respectively, in the first integral of the E-A spectrum (Figure 6b). The former peak essentially the same as the absorption peak of the 1s band of the L-phase indicating the 1s absorption band shows the first-derivative component in the E-A spectrum, which results from $\Delta\alpha$ following absorption. The latter sharp peak in the first integral of the E-A spectrum also suggests that this E-A signal results from the first derivative of the absorption band with a peak at ~22 690 cm^{-1}, although the corresponding absorption band cannot be identified in the absorption spectrum. This unknown absorption band is represented as the X_{45} band. The fact that the intensity of the first integral gradually increases as the wavenumber increases suggests that the absorption intensity of the bands higher than the X_{45} band increases in the presence of the electric field, that is, the higher bands contribute to the E-A spectrum as the zeroth derivative component. Finally, E-A and its first and second integral spectra were satisfactory simulated, as shown in Figure 6. On the basis of the simulation, the magnitude of the zeroth derivative component of each absorption band which contributes to the E-A spectrum and the magnitude of $\Delta\bar{\alpha}$ following absorption were determined. The results are shown in Table 1. As in the case of X_{295} at 295 K, the X_{45} band at 45 K is not identified in the absorption spectrum. The magnitude of $\Delta\bar{\alpha}$ for the X_{45} band shown in Table 1 (>2410 $Å^3$) was determined by assuming that this band has a Gaussian profile with fwhm ~600 cm^{-1}, and that the peak intensity of this absorption band is less than 1/5 of the observed absorption intensity at 22 690 cm^{-1}.

In ref 26, the E-A signal of the 1s band at 50 K was interpreted in terms of the red shift caused by the uniform polarizability change. This agrees with the present results, but the magnitude of change in polarizability estimated from the E-A spectra is very different from each other. The E-A signal of the band at 2.37 eV which is located in the lower energy region than the present 1s exciton band at 45 K was interpreted in terms of spectral broadening (second-derivative shape) caused by the change in polarizability which was not uniform. In the present study, the quantitative analysis of the latter band at 45 K was not carried out because of the uncertainty resulting from the weakness of the signal, but it was realized that the weak E-A signal of this band shows the shape having the second derivative of the small absorption band, as reported in ref 26. As the mechanism of the field-induced broadening of this band, the change in electric dipole moment following absorption can be considered, as in the case of the E-A spectra of the 1s exciton band at 295 K. Even at 45 K, the crystal phase which is the same as the one at room temperature still exists slightly even after the phase transition at 220 K, and this component gives the second derivative of the absorption spectrum. The PL spectra also show the coexistence of the two phases at very low temperatures, as mentioned later.

As mentioned above, the E-A signal of the 1s band is mainly originated from $\Delta\mu$ in the H-phase at room temperature and from $\Delta\alpha$ in the L-phase at low temperature. Following the phase transition caused by the conformational change of butyl ammonium chain, the interatomic transition in nature in the H-phase may be changed to the intra-atomic transition in

DOI: 10.1021/acs.jpcc.8b08116
J. Phys. Chem. C 2018, 122, 26623−26634

nature in the L-phase. The unknown absorption band, which induces very large change in polarizability, is confirmed both at room temperature and at low temperature, that is, X_{295} at 295 K and X_{45} at 45 K. In particular, the X_{45} band gives a major part of the E-A spectrum at low temperature. Our assignment of the E-A signal for this band is different from the one reported in ref 26, where the E-A signal at 2.73 eV (22 000 cm^{-1}) was assigned to the F−K oscillation. However, the square field-strength dependence both at positive and negative peaks of the strong E-A signal shown in Figure 4 clearly shows that these E-A signals mainly come from the Stark shift. These X_{295} and X_{45} absorption bands cannot be assigned clearly at the moment, but there seems to be the possibility that these bands are assigned to the 2s band.

As already mentioned, the E-A spectra observed at 45 K with different applied field strengths cross the zero line of ΔA at different wavenumbers at around 23 350 cm^{-1} (2.9 eV). This may result from the F−K oscillation, as pointed out in ref 26. Then, the band gap energy corresponding to the 1s exciton is estimated to be ∼2.9 eV. If so, the binding energy of the 1s exciton is estimated to be ∼340 meV, which is larger than the one reported in ref 26 (220 meV) by about 100 meV and smaller than the one reported in ref 48 for nanosheets of N1 crystal (490 meV). Note that the 1s exciton band is located at 20 660 cm^{-1} (2.56 eV), and that the evidence of the band gap transition could not be confirmed below 23 350 cm^{-1} in the present E-A spectra. It is stressed that the present interpretation of the E-A spectra of N1 is very similar to the one given for $(C_6H_{13}NH_3)_2PbI_4$,[25] in the sense that E-A signals around the lowest energy exciton peak at 2.34 eV (1s band) and at the step structure (2.60 eV) observed at 5 K for the layered crystal of this compound were interpreted in terms of the Stark shift and Stark broadening of the exciton bands. It is also stressed that the binding energy of the 1s exciton estimated in the present study at 45 K is very similar to the one of the 1s exciton of $(C_6H_{13}NH_3)_2PbI_4$ estimated at 5 K from the E-A and two-photon absorption spectroscopy, that is, >300 meV.[25]

PL and E-PL Measurements. PL spectrum of N1 thin films depends on temperature. The maps of the temperature-dependent PL intensity are shown in Figure 7. The PL spectra at various temperatures are shown in the Supporting Information (Figures S9 and S10). At room temperature, N1 thin films show PL emission with a peak at 525 nm. This band, which is hereafter called as the H-band, corresponds to the monolayer emission.[55] Because the sample with monolayer only was used, there was no chance for emission from higher order layers. As the temperature decreases, the H-band shows a slight blue shift, the peak intensity increases, and the bandwidth becomes narrower. At 220 K, a strong peak newly appears at 493 nm,[46] whereas the H-band becomes weaker and shows a slight blue shift by about 3 nm (see Figures 7a and S9). The newly appeared band is hereafter called as the L-band. When the temperature further decreases from 220 to 40 K, the intensity of the L-band monotonically increases, and the peak position shows a red shift by a few nanometers. As the temperature decreased below 220 K, the intensity of the H-band also increased and a slight blue shift was observed. At 40 K, it is characteristic that the H-band is much narrower than the L-band. The sudden change in PL spectra at 220 K from the H-band to the L-band is assigned to the phase transition, that is, a large lattice contraction, which is induced by the conformational change of butyl ammonium chain, as

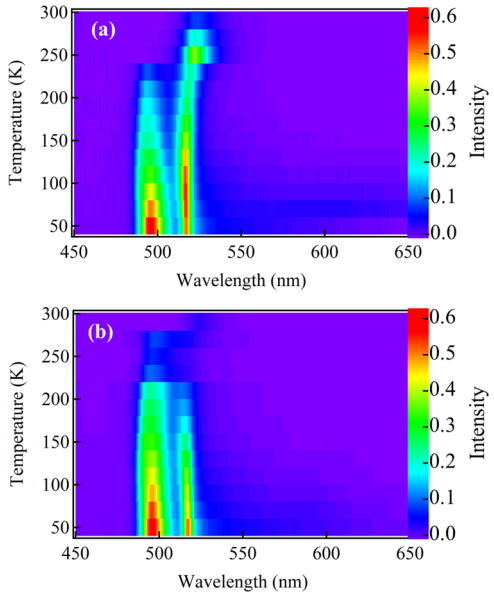

Figure 7. Map of the temperature-dependent PL intensity of N1 2D perovskites obtained by cooling from 295 K (a), and by heating from 40 K (b).

mentioned in the temperature-dependent absorption spectra. The temperature dependence of the semiconductor band gap is caused by a change in the relative position of the conduction and valence bands that usually results from dilatation (or contraction) of the lattice and from interactions of electrons with the lattice (phonon), and the band gap energy usually decreases with increasing temperature in semiconductors.[56] As known from the XRD patterns, the lattice contraction occurs in the N1 film at low temperatures. Therefore, the present result that the L-band observed at low temperatures is located in the shorter wavelength region than that of the H-band observed at high temperatures can be interpreted in terms of the lattice contraction, as in the case of usual semiconductors. In contrast with common semiconductors or the present samples of N1, which show a red shift in PL band with increasing temperature, some inorganic perovskites such as $CsPbBr_3$ nanoparticle show an enlargement in band gap as well as a blue shift in PL emission with increasing temperature,[57,58] which is considered to originate from the temperature-dependent electron−phonon coupling. It should be also noted that the map of temperature-dependent PL intensity shows a hysteresis (see Figures 7, S9 and S10) in the temperature range of 200−260 K,[55] as in the case of absorption intensity. The presence of the hysteresis in PL intensity as well as in the absorption intensity suggests that a metastable state exists between 200 and 260 K, and that the conformational structure is switchable within this temperature range.[55]

Irrespective of the peak shift, the crystal structure is regarded as the same even at different temperatures, that is, the orthorhombic phase, although a significant lattice contraction suddenly occurs at ∼220 K with decreasing temperature, as confirmed by the XRD analysis. In addition to the sharp exciton bands at 523 and 495 nm, a broad and weak emission appears at around 560 nm at low temperatures, which can be assigned to traps associated with H- and L-phases. The low-energy PL tails are considered to come from the radiative recombination of trap states, as reported in the case of 2D perovskites.[59,60] The excitonic traps do not originate from

DOI: 10.1021/acs.jpcc.8b08116
J. Phys. Chem. C 2018, 122, 26623−26634

common chemical defects but rather from the self-trapping of the band-edge excitons. The formation of self-trapped exciton results from the exciton−phonon interaction, which depends on the dimensionality of a crystalline system. Lowering the dimension of a system lowers the deformation energy, which makes self-trapping easier.[61]

As mentioned above, the bandwidth of the H-band increases with the increasing temperature. This broadening can be explained in terms of exciton interaction with phonons.[59] PbI_2 exhibits a very strong exciton-phonon coupling which leads to the existence of self-trapped excitons.[62] The exciton trapping becomes less efficient, as temperature decreases. In inorganic quantum wells, the Stokes shift is usually caused by exciton localization in the potential minima induced by the disorder.[63] By comparing PL spectra with the absorption spectra, the Stokes shift is as small as 10−20 nm (see Figure 1), suggesting a negligible influence of disorder and inhomogeneity.

The PL intensity of the peak at 495 nm increases with decreasing temperature, as shown in Figures 7, S9, and S10. The decrease of the PL intensity at high temperatures can be ascribed to the partial ionization of the exciton[17] or related to activation of another carrier recombination channel.[63] The main PL emission is intrinsic in nature with the excitonic origin at all temperatures,[48] except for the weak trap emission located at longer wavelengths.

The cooling temperature has two effects: (1) the increase of the dielectric constant because of the densification[64] and (2) some conformational changes in alkyl ammonium chains or dynamic disordering of alkyl chains, which result in structural phase transition.[65] Freezing out of vibrational and rotational modes narrows the bandwidth at low temperature. When the temperature decreased from room temperature to 40 K, the main emission band shows a blue shift by ∼30 nm, and the spectral width becomes narrower. As the temperature decreased, the PL intensity both of H-band and L-band increased monotonically (Figures 7 and S9), indicating that the nonradiative relaxation at the emitting state becomes less efficient with the decreasing temperature.

To study the relaxation dynamics of N1 in the presence of electric field following photoexcitation, we measured the E-PL spectra, that is, the field-induced change in the PL spectra. PL and E-PL spectra of N1 thin films were measured simultaneously at 295 and 45 K under vacuum conditions with an applied field strength of 0.4 MV cm^{-1}. Excitation was performed at 430 nm, where the field-induced change in absorption intensity was negligible. The results at 295 and 45 K are shown in Figures 8 and 9, respectively. As clearly shown in these figures, PL is quenched by the application of electric field, indicating that the emission quantum yield becomes smaller in the presence of the applied electric field. It is noted that the magnitude of the field-induced quenching is proportional to the square of the applied electric field at both temperatures, as shown in the Supporting Information (Figure S11). Plots of $\Delta I_{PL}/I_{PL}$ as a function of wavelength, which are given in Figures 8 and 9, show that the magnitude of the quenching is nearly the same in the whole spectral region at 295 K, whereas the value of $\Delta I_{PL}/I_{PL}$ at 45 K depends on the monitoring wavelength, for example, the field-induced quenching of the H-band at 516 nm is more efficient than that of the L-band at 495 nm (see Figure 9), clearly indicating that H-band and L-band result from different emitting states and that the efficiency of the quenching is different from each other.

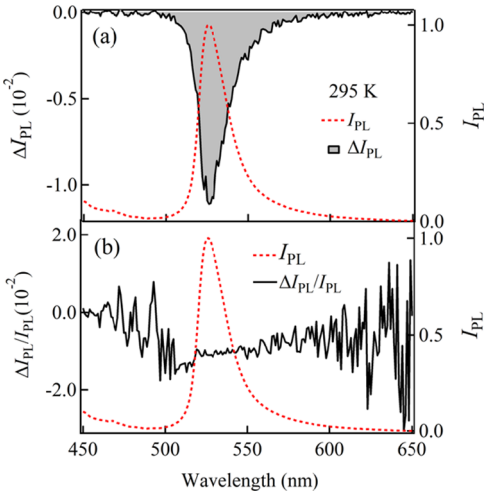

Figure 8. (a) PL and E-PL spectra of N1 obtained with the excitation at 430 nm at a temperature of 295 K with a field strength of 0.4 MV cm^{-1}, (b) ratio between E-PL spectrum and PL spectrum, that is, $\Delta I_{PL}/I_{PL}$ as a function of the monitoring wavelength and the PL spectrum. The maximum PL intensity is normalized to unity in both cases.

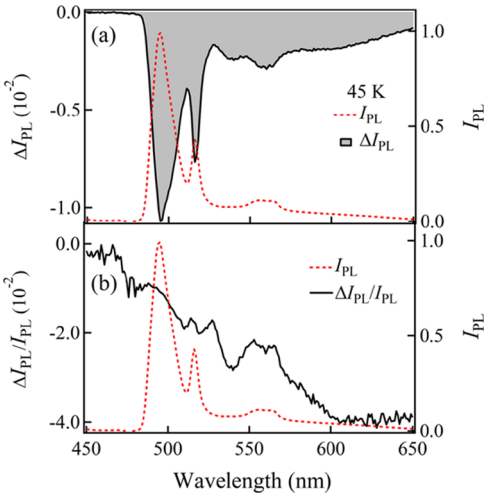

Figure 9. (a) PL and E-PL spectra of N1 obtained with excitation at 430 nm at a temperature of 45 K with a field strength of 0.4 MV cm^{-1}, (b) ratio between E-PL spectrum and PL spectrum, that is, $\Delta I_{PL}/I_{PL}$ as a function of monitoring wavelength and PL spectrum. The maximum PL intensity is normalized to unity in both cases.

From the steady-state measurements, it is not possible to confirm whether the field-induced quenching of the PL intensity comes from the change in PL lifetime or the change in population of the PL emitting state following photoexcitation. To elucidate the mechanism of the electric field effects on photoexcitation dynamics, we have measured the electric-field effects on the PL decay profile. Figure 10 shows the PL decay profiles of N1 film observed in the absence and presence of the external electric field at room temperature. Excitation and monitoring wavelengths were 430 and 525 nm, respectively. PL exhibited a multiexponential decay, and the observed decays were analyzed by assuming a triexponential decay. The results are shown in Table 2.

Besides the major component having a lifetime of ∼90 ps, a minor decaying component having a lifetime of ∼1 ns is confirmed. The difference between the decays observed at zero

DOI: 10.1021/acs.jpcc.8b08116
J. Phys. Chem. C 2018, 122, 26623−26634

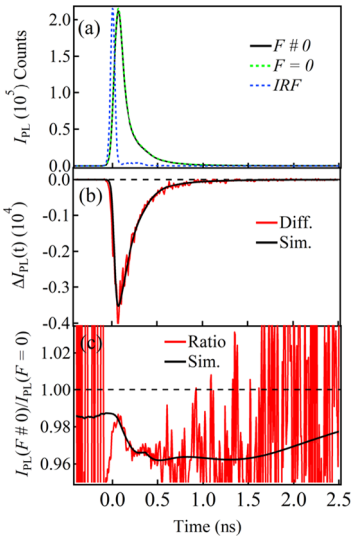

Figure 10. Electric-field effects on the PL decay profile of the N1 film. (a) Decay profiles observed at zero field and in the presence of the electric field (F), (b) difference between the decay in the presence of F and the decay at zero field, that is, $\Delta I_{PL}(t)$ ($\equiv I_{PL}(F) - I_{PL}(0)$), (c) ratio between the decay in the presence of F relative to the decay at zero fields, that is, $I_{PL}(F)/I_{PL}(0)$. The applied field strength was 0.4 MV cm^{-1}. Simulated curves are also shown in (b,c).

Table 2. Results of the Analysis of the PL Decay Profiles Observed at Zero Field ($F = 0$) and in the Presence of the Electric Field of 0.4 MV cm^{-1} ($F \neq 0$)[a]

	τ_1 (a_1)	τ_2 (a_2)	τ_3 (a_3)	τ_{av} (ns)
$F = 0$	0.090 (0.917)	0.304 (0.081)	1.065 (0.002)	0.109 (1.0)
$F \neq 0$	0.089 (0.907)	0.302 (0.079)	1.056 (0.002)	0.106 (0.988)

[a]The decays were analyzed by assuming a triexponential decay, and the lifetime of each component as well as average lifetime is shown together with the preexponential factor (in parenthesis).

fields ($I_0(t)$) and at 0.4 MV cm^{-1} ($I_{PL}(t)$), that is, $I_{PL}(t) - I_0(t)$, referred to as $\Delta I_{PL}(t)$, and the ratio $I_{PL}(t)/I_0(t)$ ($\equiv I_{PL}(F \neq 0)/I_{PL}(F = 0)$ in Figure 10) are shown in Figure 10b,c, respectively. The integrated intensity of $\Delta I_{PL}(t)$ shown in Figure 10b is negative, indicating the field-induced quenching, in agreement with the steady-state E-PL spectra shown in Figure 8. Further, the ratio $I_{PL}(t)/I_0(t)$ is less than unity at t = 0 (see Figure 10c), indicating that there is a reduction in population of the emitting state in the presence of electric field. Furthermore, this ratio decreases as a function of time, t, indicating that the PL lifetime decreases in the presence of electric field. In fact, a small decrease both in lifetime and in the pre-exponential factor in the presence of the electric field is evaluated by the simulation of decay profiles, as shown in Table 2. In the results, it is known that the average lifetime, defined by $\sum A_i\tau_i/\sum A_i$, becomes shorter in the presence of electric field and that the population of the emitting state of N1 following photoexcitation is decreased by the application of electric field. Thus, the nonradiative decay rate at the emitting state of N1 is enhanced by the applied electric field.

At room temperature, it is considered that PL is emitted from a single state. At low temperatures such as 45 K, on the other hand, PL emissions resulting from different emitting states were observed, that is, H-band and L-band. As already mentioned, both bands show field-induced quenching whose efficiency is different from each other. Further, the bands located in the longer wavelength region, which are assigned to the trap emission, show more efficient field-induced quenching than that of the exciton band. Then, it is suggested that the relaxation to the trap state following photoexcitation is decelerated by the application of an electric field. Here, we have to confess that the efficiency of the field-induced quenching of H-band and L-band at low temperatures depends on the sample condition. As shown in Figure 9, the field-induced quenching of the H-band is more efficient than that of the L-band. This is the usual case, but the relation becomes opposite depending on the sample, that is, the L-band shows more efficient field-induced quenching than that of the H-band, as shown in the Supporting Information (Figure S11). However, it should be noted that the field-induced quenching of the trap emission located in the longer wavelength region is always more efficient than the exciton emissions which give H- and L-bands (see Figures 9 and S12).

CONCLUSIONS

Absorption, PL, E-A, and E-PL spectra of solid thin films of two-dimensional hybrid organic−inorganic halide perovskite, $(C_4H_9NH_3)_2PbI_4$ (N1), have been measured at various temperatures in the range of 40−300 K. A structural phase transition occurs at 200−260 K because of the butyl ammonium chain rearrangement, and hysteresis was observed in the measurements of the maps of temperature-dependent absorption intensity and PL intensity, indicating the presence of metastable state in this temperature range. The E-A spectra observed at 295 and 45 K were analyzed with the integral method by assuming that the electric-field effects on the absorption spectra result both from the Stark shift and from the field-induced change in absorption intensity. In the results, the magnitude of $\Delta\bar{\alpha}$ and $|\Delta\boldsymbol{\mu}|$ were determined. The strong signal observed in the E-A spectra at 45 K, which cannot be corresponded to the observed absorption band, is assigned to the one resulting from the Stark shift of very weak absorption band. The binding energy of the 1s exciton of N1 film is estimated to be ≥300 meV at 45 K, and the weak absorption band which gives the large Stark shift may be assigned to the 2s exciton band. The presence of the absorption band which cannot be identified in the absorption spectra is also suggested at 295 K to interpret the observed E-A spectrum. The E-PL spectra show that PL of N1 is quenched by the application of electric field both at room temperature and at a low temperature of 45 K, where two exciton emissions show different efficiency in field-induced quenching from each other. At low temperatures, not only the exciton emissions but also the trap emissions are observed, and it is found that the efficiency of the field-induced quenching of the trap emissions is much higher than those of the exciton emissions. The field-induced change in the PL decay curve shows that the field-induced quenching results from the field induced decrease both in population of the emitting state, following photo-excitation, and in field-induced shortening of the PL lifetime, which results from the field-induced enhancement of the nonradiative decay rate at the emitting state.

ASSOCIATED CONTENT

Supporting Information

The Supporting Information is available free of charge on the ACS Publications website at DOI: 10.1021/acs.jpcc.8b08116.

DOI: 10.1021/acs.jpcc.8b08116
J. Phys. Chem. C 2018, 122, 26623−26634

Temperature-dependent absorption spectra, E-A spectra observed at the second harmonic of the modulation frequency with different applied field strengths, E-A spectra analyzed by the differential method, E-A spectra observed at the first harmonic of the modulation frequency, temperature-dependent PL spectra, applied field strength dependence of the PL intensity, and E-PL spectrum of N1 at low temperature (PDF)

AUTHOR INFORMATION

Corresponding Authors

*E-mail: diau@mail.nctu.edu.tw (E.W.-G.D.).
*E-mail: nohta@nctu.edu.tw (N.O.).

ORCID

Eric Wei-Guang Diau: 0000-0001-6113-5679
Nobuhiro Ohta: 0000-0003-4255-6448

Author Contributions

‖V.K. and K.A. contributed equally to this work.

Notes

The authors declare no competing financial interest.

ACKNOWLEDGMENTS

The Ministry of Science and Technology (MOST) in Taiwan provided the financial support of this research (106-2811-M-009-018 and 107-3017-F009-003). This work was also financially supported by the Center for Emergent Functional Matter Science of National Chiao Tung University from The Featured Areas Research Center Program within the framework of the Higher Education Sprout Project by the Ministry of Education (MOE) in Taiwan.

REFERENCES

(1) Saliba, M.; Matsui, T.; Domanski, K.; Seo, J.-Y.; Ummadisingu, A.; Zakeeruddin, S. M.; Correa-Baena, J.-P.; Tress, W. R.; Abate, A.; Hagfeldt, A.; Gratzel, M. Incorporation of Rubidium Cations into Perovskite Solar Cells Improves Photovoltaic Performance. *Science* **2016**, *354*, 206−209.

(2) Saliba, M.; Matsui, T.; Seo, J.-Y.; Domanski, K.; Correa-Baena, J.-P.; Nazeeruddin, M. K.; Zakeeruddin, S. M.; Tress, W.; Abate, A.; Hagfeldt, A.; Grätzel, M. Cesium-Containing Triple Cation Perovskite Solar Cells: Improved Stability, Reproducibility and High Efficiency. *Energy Environ. Sci.* **2016**, *9*, 1989−1997.

(3) Gao, P.; Grätzel, M.; Nazeeruddin, M. K. Organohalide Lead Perovskites for Photovoltaic Applications. *Energy Environ. Sci.* **2014**, *7*, 2448−2463.

(4) Pellet, N.; Gao, P.; Gregori, G.; Yang, T.-Y.; Nazeeruddin, M. K.; Maier, J.; Grätzel, M. Mixed-Organic-Cation Perovskite Photovoltaics for Enhanced Solar-Light Harvesting. *Angew. Chem., Int. Ed.* **2014**, *53*, 3151−3157.

(5) Eperon, G. E.; Stranks, S. D.; Menelaou, C.; Johnston, M. B.; Herz, L. M.; Snaith, H. J. Formamidinium Lead Trihalide: A Broadly Tunable Perovskite for Efficient Planar Heterojunction Solar Cells. *Energy Environ. Sci.* **2014**, *7*, 982−988.

(6) Pang, S.; Hu, H.; Zhang, J.; Lv, S.; Yu, Y.; Wei, F.; Qin, T.; Xu, H.; Liu, Z.; Cui, G. NH2CHNH2PbI3: An Alternative Organolead Iodide Perovskite Sensitizer for Mesoscopic Solar Cells. *Chem. Mater.* **2014**, *26*, 1485−1491.

(7) Hao, F.; Stoumpos, C. C.; Cao, D. H.; Chang, R. P. H.; Kanatzidis, M. G. Lead-free solid-state organic-inorganic halide perovskite solar cells. *Nat. Photonics* **2014**, *8*, 489−494.

(8) Ogomi, Y.; Morita, A.; Tsukamoto, S.; Saitho, T.; Fujikawa, N.; Shen, Q.; Toyoda, T.; Yoshino, K.; Pandey, S. S.; Ma, T.; Hayase, S. $CH_3NH_3Sn_xPb_{(1-x)}I_3$ Perovskite Solar Cells Covering up to 1060 nm. *J. Phys. Chem. Lett.* **2014**, *5*, 1004−1011.

(9) Snaith, H. J. Perovskites: The Emergence of a New Era for Low-Cost, High-Efficiency Solar Cells. *J. Phys. Chem. Lett.* **2013**, *4*, 3623−3630.

(10) Hirasawa, M.; Ishihara, T.; Goto, T. Exciton Features in 0-, 2-, and 3-Dimensional Networks of $[PbI_6]_4$- Octahedra. *J. Phys. Soc. Jpn.* **1994**, *63*, 3870−3879.

(11) Tanaka, K.; Kondo, T. Bandgap and exciton binding energies in lead-iodide-based natural quantum-well crystals. *Sci. Technol. Adv. Mater.* **2003**, *4*, 599−604.

(12) Mao, L.; Tsai, H.; Nie, W.; Ma, L.; Im, J.; Stoumpos, C. C.; Malliakas, C. D.; Hao, F.; Wasielewski, M. R.; Mohite, A. D.; Kanatzidis, M. G. Role of Organic Counterion in Lead- and Tin-Based Two-Dimensional Semiconducting Iodide Perovskites and Application in Planar Solar Cells. *Chem. Mater.* **2016**, *28*, 7781−7792.

(13) Blancon, J.-C.; Tsai, H.; Nie, W.; Stoumpos, C. C.; Pedesseau, L.; Katan, C.; Kepenekian, M.; Soe, C. M. M.; Appavoo, K.; Sfeir, M. Y.; Tretiak, S.; Ajayan, P. M.; Kanatzidis, M. G.; Even, J.; Crochet, J. J.; Mohite, A. D. Extremly Efficient Internal Exciton Dissociation through Edge States in Layered 2D Perovskites. *Science* **2017**, *355*, 1288−1292.

(14) Mitzi, D. B.; Liang, K. Preparation and Properties of $(C_4H_9NH_3)_2EuI_4$: A Luminescent Organic−Inorganic Perovskite with a Divalent Rare-Earth Metal Halide Framework. *Chem. Mater.* **1997**, *9*, 2990−2995.

(15) Keldysh, L. Coulomb Interaction in Thin Semiconductor and Semimetal Films. *JETP Lett.* **1979**, *29*, 658−660.

(16) Hanamura, E.; Nagaosa, N.; Kumagai, M.; Takagahara, T. Quantum Wells with Enhanced Exciton Effects and Optical Non-Linearity. *Mater. Sci. Eng., B* **1988**, *1*, 255−258.

(17) Hong, X.; Ishihara, T.; Nurmikko, A. V. Dielectric Confinement Effect on Excitons in PbI_4-Based Layered Semiconductors. *Phys. Rev. B: Condens. Matter Mater. Phys.* **1992**, *45*, 6961−6964.

(18) Ishihara, T.; Takahashi, J.; Goto, T. Exciton State in Two-Dimensional Perovskite Semiconductor (C10H21NH3)2PbI4. *Solid State Commun.* **1989**, *69*, 933−936.

(19) Kagan, C. R.; Mitzi, D. B.; Dimitrakopoulos, C. Organic-Inorganic Hybrid Materials as Semiconducting Channels in Thin-Film Field-Effect Transistors. *Science* **1999**, *286*, 945−947.

(20) Dou, L.; Wong, A. B.; Yu, Y.; Lai, M.; Kornienko, N.; Eaton, S. W.; Fu, A.; Bischak, C. G.; Ma, J.; Ding, T.; Ginsberg, N. S.; Wang, L.-W.; Alivisatos, A. P.; Yang, P. Atomically Thin Two-Dimensional Organic-Inorganic Hybrid Perovskites. *Science* **2015**, *349*, 1518−1521.

(21) Cao, D. H.; Stoumpos, C. C.; Farha, O. K.; Hupp, J. T.; Kanatzidis, M. G. 2D Homologous Perovskites as Light-Absorbing Materials for Solar Cell Applications. *J. Am. Chem. Soc.* **2015**, *137*, 7843−7850.

(22) Zhou, J.; Chu, Y.; Huang, J. Photodetectors Based on Two-Dimensional Layer-Structured Hybrid Lead Iodide Perovskite Semiconductors. *ACS Appl. Mater. Interfaces* **2016**, *8*, 25660−25666.

(23) Zhang, X.; Ren, X.; Liu, B.; Munir, R.; Zhu, X.; Yang, D.; Li, J.; Liu, Y.; Smilgies, D.-M.; Li, R.; Yang, Z.; Niu, T.; Wang, X.; Amassian, A.; Zhao, K.; Liu, S. Stable High Efficiency Two-Dimensional Perovskite Solar Cells via Cesium Doping. *Energy Environ. Sci.* **2017**, *10*, 2095−2102.

(24) Tanaka, K.; Takahashi, T.; Kondo, T.; Umeda, K.; Ema, K.; Umebayashi, T.; Asai, K.; Uchida, K.; Miura, N. Electronic and Excitonic Structures of Inorganic−Organic Perovskite-Type Quantum-Well Crystal $(C_4H_9NH_3)_2PbBr_4$. *Jpn. J. Appl. Phys.* **2005**, *44*, 5923−5932.

(25) Tanaka, K.; Sano, F.; Takahashi, T.; Kondo, T.; Ito, R.; Ema, K. Two-Dimensional Wannier Excitons in a Layered-Perovskite-Type Crystal (C6H13NH3)2PbI4. *Solid State Commun.* **2002**, *122*, 249−252.

(26) Amerling, E.; Baniya, S.; Lafalce, E.; Zhang, C.; Vardeny, Z. V.; Whittaker-Brooks, L. Electroabsorption Spectroscopy Studies of $(C_4H_9NH_3)_2PbI_4$ Organic−Inorganic Hybrid Perovskite Multiple Quantum Wells. *J. Phys. Chem. Lett.* **2017**, *8*, 4557−4564.

DOI: 10.1021/acs.jpcc.8b08116
J. Phys. Chem. C 2018, 122, 26623−26634

(27) Roiati, V.; Mosconi, E.; Listorti, A.; Colella, S.; Gigli, G.; De Angelis, F. Stark Effect in Perovskite/TiO2 Solar Cells: Evidence of Local Interfacial Order. *Nano Lett.* **2014**, *14*, 2168−2174.
(28) Wu, X.; Yu, H.; Li, L.; Wang, F.; Xu, H.; Zhao, N. Composition-Dependent Light-Induced Dipole Moment Change in Organometal Halide Perovskites. *J. Phys. Chem. C* **2015**, *119*, 1253−1259.
(29) Legaspi, C. M.; Peteanu, L. A.; Yaron, D. J. Modeling Field-Induced Quenching in Poly(p-phenylene vinylene) Polymers and Oligomers. *J. Phys. Chem. B* **2015**, *119*, 7625−7634.
(30) Ziffer, M. E.; Mohammed, J. C.; Ginger, D. S. Electroabsorption Spectroscopy Measurements of the Exciton Binding Energy, Electron−Hole Reduced Effective Mass, and Band Gap in the Perovskite $CH_3NH_3PbI_3$. *ACS Photonics* **2016**, *3*, 1060−1068.
(31) Leijtens, T.; Kandada, A. R. S.; Eperon, G. E.; Grancini, G.; D'Innocenzo, V.; Ball, J. M.; Stranks, S. D.; Snaith, H. J.; Petrozza, A. Modulating the Electron-Hole Interaction in a Hybrid Lead Halide Perovskite with an Electric Filed. *J. Am. Chem. Soc.* **2015**, *137*, 15451−15459.
(32) Awasthi, K.; Du, K.-B.; Wang, C.-Y.; Tsai, C.-L.; Hamada, M.; Narra, S.; Diau, E. W.-G.; Ohta, N. Electroabsorption Studies of Multi-Colored Lead Halide Perovskite Nanocrystalline Solid Films. *ACS Photonics* **2018**, *5*, 2408−2417.
(33) Ruf, F.; Magin, A.; Schultes, M.; Ahlswede, E.; Kalt, H.; Hetterich, M. Excitonic Nature of Optical Transitions in Electroabsortpion Spectra of Perovskite Solar Cells. *Appl. Phys. Lett.* **2018**, *112*, 083902.
(34) Ohta, N. Electric Field Effects on Photochemical Dynamics in Solid Films. *Bull. Chem. Soc. Jpn.* **2002**, *75*, 1637−1655.
(35) Jalviste, E.; Ohta, N. Theoretical Foundation of Electroabsorption Spectroscopy: Self-Contained Derivation of the Basic Equations with the Direction Cosine Method and the Euler Angle Method. *J. Photochem. Photobiol., C* **2007**, *8*, 30−46.
(36) Ohta, N.; Awasthi, K.; Okoshi, K.; Manseki, K.; Miura, H.; Inoue, Y.; Nakamura, K.; Kono, H.; Diau, E. W.-G. Stark Spectroscopy of Absorption and Emission of Indoline Sensitizers: A Correlation with the Performance of Photovoltaic Cells. *J. Phys. Chem. C* **2016**, *120*, 26206−26216.
(37) Awasthi, K.; Wang, C.-Y.; Fathi, A.; Narra, S.; Diau, E. W.-G.; Ohta, N. Anisotropic Electric Field Effect on the Photoluminescence of CH3NH3PbI3 Perovskite Sandwiched between Conducting and Insulating Films. *J. Phys. Chem. C* **2017**, *121*, 22700−22706.
(38) Awasthi, K.; Iimori, T.; Ohta, N. Electroabsorption Spectra of Quantum Dots of PbS and Analysis by the Integral Method. *J. Phys. Chem. C* **2015**, *119*, 4351−4361.
(39) Awasthi, K.; Iimori, T.; Ohta, N. Integral Method Analysis of Electroabsorption Spectra and Its Application to Quantum Dots of PbSe. *J. Phys. Chem. C* **2014**, *118*, 18170−18176.
(40) Stoumpos, C. C.; Cao, D. H.; Clark, D. J.; Young, J.; Rondinelli, J. M.; Jang, J. I.; Hupp, J. T.; Kanatzidis, M. G. Ruddlesden−Popper Hybrid Lead Iodide Perovskite 2D Homologous Semiconductors. *Chem. Mater.* **2016**, *28*, 2852−2867.
(41) Umeuchi, S.; Nishimura, Y.; Yamazaki, I.; Murakami, H.; Yamashita, M.; Ohta, N. Electric Field Effects on Absorption and Fluorescence Spectra of Pyrene Doped in a PMMA Polymer Film. *Thin Solid Films* **1997**, *311*, 239−245.
(42) Ishihara, T.; Takahashi, J.; Goto, T. Optical Properties due to Electronic Transitions in Two-Dimensional Semiconductors (CnH2n+1NH3)2PbI4. *Phys. Rev. B: Condens. Matter Mater. Phys.* **1990**, *42*, 11099−11107.
(43) Kataoka, T.; Kondo, T.; Ito, R.; Sasaki, S.; Uchida, K.; Miura, N. Magneto-Optical Study on Excitonic Spectra in (C6H13NH3)-2PbI4. *Phys. Rev. B: Condens. Matter Mater. Phys.* **1993**, *47*, 2010−2018.
(44) Ishihara, T.; Hirasawa, M.; Goto, T. Optical Properties and Electronic Structures of Self-Organized Quantum Well $(C_nH_{2n+1}NH_3)_2PbX_4$ (X= I, Br, Cl). *Jpn. J. Appl. Phys.* **1995**, *34*, 71.
(45) Kind, R. Structural Phase Transitions in Perovskite Layer Structures. *Ferroelectrics* **1980**, *24*, 81−88.
(46) Dolzhenko, Y. I.; Inabe, T.; Maruyama, Y. In Situ X-Ray Observation on the Intercalation of Weak Interaction Molecules into Perovskite-Type Layered Crystals $(C_9H_{19}NH_3)_2PbI_4$ ad $(C_{10}H_{21}NH_3)_2CdCl_4$. *Bull. Chem. Soc. Jpn.* **1986**, *59*, 563−567.
(47) Wu, X.; Trinh, M. T.; Niesner, D.; Zhu, H.; Norman, Z.; Owen, J. S.; Yaffe, O.; Kudisch, B. J.; Zhu, X.-Y. Trap States in Lead Iodide Perovskites. *J. Am. Chem. Soc.* **2015**, *137*, 2089−2096.
(48) Yaffe, O.; Chernikov, A.; Norman, Z. M.; Zhong, Y.; Velauthapillai, A.; van der Zande, A.; Owen, J. S.; Heinz, T. F. Excitons in Ultrathin Organic-Inorganic Perovskite Crystals. Phys. *Phys. Rev. B: Condens. Matter Mater. Phys.* **2015**, *92*, 045414.
(49) Billing, D. G.; Lemmerer, A. Synthesis, Characterization and Phase Transitions of the Inorganic−Organic Layered Perovskite-Type Hybrids $[(C_nH_{2n+1}NH_3)_2PbI_4]$(n= 12, 14, 16 and 18). *New J. Chem.* **2008**, *32*, 1736−1746.
(50) Aspnes, D. E. Modulation Spectroscopy/Electric Field Effects on the Dielectric Function of Semiconductors. In *Handbook on Semiconductors*; Balkanski, M., Ed.; North-Holland: Amsterdam, 1980; Vol. *2*, pp 109−154.
(51) Liptay, W. Dipole Moments and Polarizabilities of Molecules in Excited Electronic States. In *Excited States*; Lim, E. C., Ed.; Academic Press: New York, 1974; Vol. *1*, pp 129−229.
(52) Bublitz, G. U.; Boxer, S. G. Stark Spectroscopy: Applications in Chemistry, Biology, and Materials Science. *Annu. Rev. Phys. Chem.* **1997**, *48*, 213−242.
(53) Locknar, S. A.; Peteanu, L. A. Investigation of the Relationship between Dipolar Properties and Cis−Trans Configuration in Retinal Polyenes: A Comparative Study Using Stark Spectroscopy and Semiempirical Calculations. *J. Phys. Chem. B* **1998**, *102*, 4240−4246.
(54) Shimizu, M.; Fujisawa, J.-I.; Ishi-Hayase, J. Influence of Dielectric Confinement on Excitonic Nonlinearity in Inorganic-Organic Layered Semiconductors. *Phys. Rev. B: Condens. Matter Mater. Phys.* **2005**, *71*, 205306.
(55) Ni, L.; Huynh, U.; Cheminal, A.; Thomas, T. H.; Shivanna, R.; Hinrichsen, T. F.; Ahmad, S.; Sadhanala, A.; Rao, A. Real-Time Observation of Exciton−Phonon Coupling Dynamics in Self-Assembled Hybrid Perovskite Quantum Wells. *ACS Nano* **2017**, *11*, 10834−10843.
(56) Varshni, Y. P. Temperature Dependence of the Energy Gap in Semiconductors. *Physica* **1967**, *34*, 149−154.
(57) Li, J.; Yuan, X.; Jing, P.; Li, J.; Wei, M.; Hua, J.; Zhao, J.; Tian, L. Temperature-Dependent Photoluminescence of Inorganic Perovskite Nanocrystal Film. *RSC Adv.* **2016**, *6*, 78311−78316.
(58) Tong, Y.; Bohn, B. J.; Bladt, E.; Wang, K.; Müller-Buschbaum, P.; Bals, S.; Urban, A. S.; Polavarapu, L.; Feldmann, J. From Precursor Powders to $CsPbX_3$ Perovskite Nanowires: One Pot Synthesis, Growth Mechanism, and Self-Assembly. *Angew. Chem., Int. Ed.* **2017**, *56*, 13887−13892.
(59) Gauthron, K.; Lauret, J.-S.; Doyennette, L.; Lanty, G.; Al Choueiry, A.; Zhang, S. J.; Brehier, A.; Largeau, L.; Mauguin, O.; Bloch, J.; Deleporte, E. Optical Spectroscopy of Two-Dimensional Layered $(C_6H_5C_2H_4\text{-}NH_3)_2\text{-}PbI_4$ Perovskite. *Opt. Express* **2010**, *18*, 5912−5919.
(60) Wu, X.; Trinh, M. T.; Niesner, D.; Zhu, H.; Norman, Z.; Owen, J. S.; Yaffe, O.; Kudisch, B. J.; Zhu, X.-Y. Trap States in Lead Halide Perovskites. *J. Am. Chem. Soc.* **2015**, *137*, 2089−2096.
(61) Song, K. S.; Williams, R. T. Self-trapped Excitons. In *Springer Series in Solid-State Sciences*; Springer: Berlin, 1993, Vol. *105*.
(62) Lee, J.; Koteles, E. S.; Vassell, M. O. Luminescence Linewidths of Excitons in GaAs Quantum Wells below 150 K. *Phys. Rev. B: Condens. Matter Mater. Phys.* **1986**, *33*, 5512−5516.
(63) Plekhanov, V. G. Lead Halides: Electronic Properties and Applications. *Prog. Mater. Sci.* **2004**, *49*, 787−886.
(64) Grell, M.; Bradley, D. D. C.; Ungar, G.; Hill, J.; Whitehead, K. S. Interplay of Physical Structure and Photophysics for a Liquid Crystalline Polyfluorene. *Macromolecules* **1999**, *32*, 5810−5817.
(65) Abid, H.; Trigui, A.; Mlayah, A.; Hlil, E. K.; Abid, Y. Phase Transition in Organic−Inorganic Perovskite $(C_9H_{19}NH_3)_2PbI_2Br_2$ of Long-Chain Alkylammonium. *Results Phys.* **2012**, *2*, 71−76.

DOI: 10.1021/acs.jpcc.8b08116
J. Phys. Chem. C 2018, 122, 26623−26634